View metadata, citation and similar papers at core.ac.uk

brought to you by CORE

provided by Research Online

University of Wollongong

Research Online

Faculty of Engineering - Papers (Archive)

Faculty of Engineering and Information Sciences

1-1-2011

Structural, dielectric, antiferromagnetic, and thermal properties of the frustrated hexagonal Ho1-xErxMnO3 manganites

Peng Liu
University of Wollongong, pl990@uowmail.edu.au

Xiaolin Wang
University of Wollongong, xiaolin@uow.edu.au

Zhenxiang Cheng
University of Wollongong, cheng@uow.edu.au

Yi Du
University of Wollongong, ydu@uow.edu.au

Hideo Kimura
National Institute For Materials Science

Follow this and additional works at: https://ro.uow.edu.au/engpapers

 Part of the Engineering Commons

https://ro.uow.edu.au/engpapers/1356

Recommended Citation

Liu, Peng; Wang, Xiaolin; Cheng, Zhenxiang; Du, Yi; and Kimura, Hideo: Structural, dielectric, antiferromagnetic, and thermal properties of the frustrated hexagonal Ho1-xErxMnO3 manganites 2011, 1-8.
https://ro.uow.edu.au/engpapers/1356

Research Online is the open access institutional repository for the University of Wollongong. For further information contact the UOW Library: research-pubs@uow.edu.au

Structural, dielectric, antiferromagnetic, and thermal properties of the frustrated hexagonal $Ho_{1-x}Er_xMnO_3$ manganites

Peng Liu,[1] Xiao-Lin Wang,[1,*] Zhen-Xiang Cheng,[1] Yi Du,[1] and Hideo Kimura[2]

[1]*Institute for Superconducting and Electronic Materials, Faculty of Engineering, University of Wollongong, Squaire Way, North Wollongong, New South Wales 2500, Australia*

[2]*Crystal Science and Technology Group, National Institute for Materials Science, 1-2-1 Sengen, Tsukuba, Ibaraki 305-0047, Japan*

(Received 20 September 2010; revised manuscript received 20 December 2010; published 6 April 2011)

The Er doping effects on the structural, dielectric, ferroelectric, magnetic, and thermal properties of the hexagonal $Ho_{1-x}Er_xMnO_3$ ($0 \leqslant x \leqslant 1$) compounds synthesized by the solid-state reaction method have been investigated by Rietveld refinement and by measurements of dielectric constant, ferroelectric hysteresis loops, magnetic susceptibility, and specific heat. The *a* lattice parameter decreases as the Er content increases, whereas the *c* lattice parameter nearly keeps constant with pretty minor fluctuations. Dielectric data and ferroelectric hysteresis loops show all the samples are not only ferroelectric materials with leaky nature, but also with dielectric relaxation related to oxygen vacancies. The magnetizations of these compounds gradually decrease with increasing Er content. The Mn^{3+} ions in each sample remain stable in the high-spin state in the Mn-O_5 trigonal bipyramidal crystal field. Specific heat measurements show that the antiferromagnetic transition temperature continuously rises from 72 K for $HoMnO_3$ to 76 K for $ErMnO_3$. The Debye temperatures are 381 K for $ErMnO_3$ and 422 K for $HoMnO_3$.

DOI: 10.1103/PhysRevB.83.144404 PACS number(s): 75.47.Lx, 77.55.Nv, 77.22.−d, 65.40.Ba

I. INTRODUCTION

Rare-earth manganites, $RMnO_3$, possess two phases according to the ionic radii of the rare-earth elements. The compounds with small atoms (R = Ho to Lu, Y, and Sc) crystallize in the hexagonal structure, while the others with large-R atoms (R = La to Dy) crystallize in the orthorhombic phase. Since ferroelectricity can only be observed in the hexagonal manganites with the noncentrosymmetric $p6_3cm$ space group, these compounds have attracted great interest due to the coupling between ferroelectric and antiferromagnetic orderings.[1,2] The strong coupling allows magnetization and electrical polarization to be mutually controlled in an external electrical field and an external magnetic field, respectively. The novel property makes such multiferroic compounds promising in potential applications, such as spintronics devices, multistate memory storage, transducers, actuators, and magnetoelectric sensors.[3,4]

The hexagonal $RMnO_3$ compounds show ferroelectric transitions (T_C) at high temperatures in the range of 590–1000 K and antiferromagnetic transitions (T_N) at low temperatures from 70 to 130 K.[5,6] Their crystal structures are constructed alternatively from two layers along the *c* axis. One layer consists of the corner-sharing Mn-O_5 trigonal bipyramids, where Mn^{3+} ions are encompassed by three in-plane oxygen ions and two apical oxygen ions.[7] The other layer comprises eightfold coordinated rare-earth ions with two symmetric sites. The hexagonal $RMnO_3$ compounds are characterized by the frustrated triangular magnetic structure of the Mn^{3+} moments in the *ab* plane, with neighboring Mn spins rotated by 120°.[5] Mn^{3+} ions are antiferromagnetically coupled below T_N by Mn-O-Mn superexchange interactions through in-plane oxygen ions. The ferroelectric ordering along the *c* axis is attributed to two kinds of anti-parallel electric dipoles produced by the R-O displacements.[8]

The hexagonal $HoMnO_3$ and $ErMnO_3$ individually have similar antiferromagnetic transitions at 72 and 76 K. However, their ferroelectric transition temperatures have a large difference, 875 K for $HoMnO_3$ and 525 K for $ErMnO_3$.[9,10] The coupling between antiferromagnetic and ferroelectric orderings has been proved by magnetic field dependence of ferroelectric polarization below antiferromagnetic transition temperature.[11] In addition, $HoMnO_3$ exhibits spin reorientation of Mn^{3+} ions at 33 K and antiferromagnetic ordering of Ho^{3+} ions below around 5 K.[12] However, there is only one magnetic transition below 5 K in $ErMnO_3$ due to the ferrimagnetic ordering of Er^{3+} spins.[13]

Despite the crystal structures of $HoMnO_3$ and $ErMnO_3$ are quite similar, the mutual doping in $Ho_{1-x}Er_xMnO_3$ provides a chance to investigate additional contributions to the doping effects. Especially, large differences in ferroelectric transitions make it significant to investigate how the ferroelectric and dielectric properties are modified through mutual doping between $HoMnO_3$ and $ErMnO_3$. Zhou *et al.* reported the magnetic phase diagram of the $Ho_{1-x}Er_xMnO_3$ system with a maximum doping level of $x = 0.4$ by studying the specific heat and the dielectric constant at low temperatures.[14] The aim of this work is to investigate how the mutual doping affects crystal structures, antiferromagnetic states, as well as the thermal and ferroelectric properties of the $Ho_{1-x}Er_xMnO_3$ system. The investigated doping levels of this system have been extended up to $x = 1$. Moreover, the high temperature dielectric properties have been particularly examined. It is found that all the samples are ferroelectric materials that possess a dielectric relaxation process caused by oxygen vacancies.

II. EXPERIMENT

Polycrystalline samples of $Ho_{1-x}Er_xMnO_3$ ($0 \leqslant x \leqslant 1$) were synthesized by the conventional solid-state reaction method, using Ho_2O_3, Er_2O_3, and $MnCO_3$ with purity of 99.9% as starting materials. Stoichiometric mixtures of these compounds were ground thoroughly, hydrostatically pressed into a pellet, and annealed in air at 1000 °C for 16 h. After

 ©2011 American Physical Society

a second grinding, the resulting powder was compressed into a pellet again. The final sintering was carried out in air at 1200 °C for 24 h. The X-ray diffraction (XRD) patterns of all samples were obtained by a GBC-MMA diffractometer using Cu Kα radiation ($\lambda = 1.54059$ Å). Rietveld refinement of the XRD data was carried out using the Rietica program. The magnetic properties were examined on a physical properties measurement system (PPMS, Quantum Design), using a vibrating sample magnetometer. Magnetic susceptibility data were collected between 5 and 300 K at a magnetic field of 1000 Oe under both zero-field-cooled (ZFC) and field-cooled (FC) process. The specific heat capacity was obtained without magnetic fields by using the specific heat option in PPMS. The dielectric properties of pellets that were coated with gold as electrodes were measured from 350 to 800 K within the frequency range from 10 to 100 kHz by utilizing an HP 4284A LCR meter. Ferroelectric hysteresis loops were measured at room temperature with the frequency of 1 kHz using an aixACCT TF 2000 ferroelectric tester.

III. RESULTS AND DISCUSSION

The samples with the composition of $x = 0-0.4$ and $0.7-1$ are all in single phase. As can be seen in Fig. 1, each XRD reflection peak can be indexed according to the hexagonal structure with the $P6_3cm$ space group, in agreement with previous reports.[15,16] The diffraction peaks are quite distinct and shift to higher angles with increasing Er doping levels. The XRD peak splitting of the $Ho_{1-x}Er_xMnO_3$ samples with $x = 0.5$ and 0.6 at 51.5° and 61.5° indicates the coexistence of $ErMnO_3$ and $HoMnO_3$ phases, which is also confirmed later by two transition peaks at 72 and 76 K in the specific heat data. Zhou *et al.*[14] investigated the magnetic phase diagram of single-crystalline $Ho_{1-x}Er_xMnO_3$ samples with a maximum doping level of only $x = 0.4$, greatly supporting our observations that the mixed-phase samples with $x = 0.5$ and 0.6 show distinctive chemical phase separation. The chemical immiscibility is likely despite of the small differences in the sizes between Ho^{3+} and Er^{3+} ions. The Rietveld refinement method was used to refine the XRD patterns of all single-phase compounds. The goodness of fit of $Ho_{0.3}Er_{0.7}MnO_3$ is shown

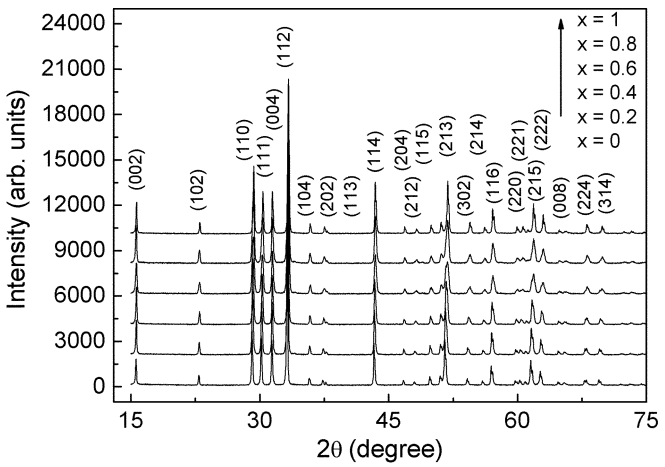

FIG. 1. The room temperature XRD patterns of $Ho_{1-x}Er_xMnO_3$ ($x = 0$, 0.2, 0.4, 0.6, 0.8, 1) as representative samples.

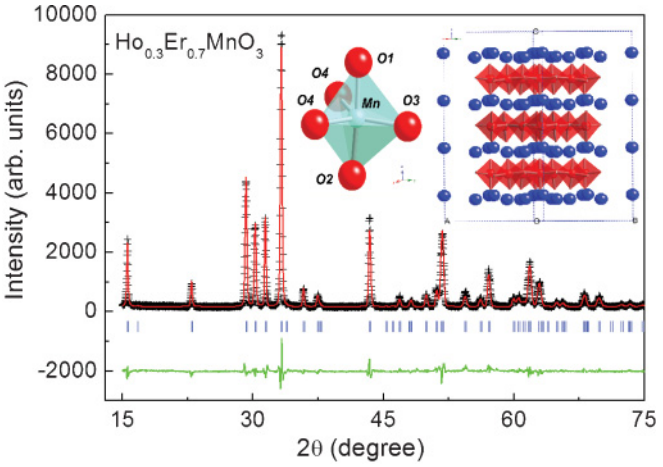

FIG. 2. (Color online) Rietveld refinement results on the XRD pattern of the $Ho_{0.3}Er_{0.7}MnO_3$ sample. The cross marks and red line are the experimental pattern and the calculated pattern, respectively. The blue vertical marks are the peak positions of Bragg diffraction. The green line at the bottom is the difference between the experimental pattern and the calculated pattern. $R_P = 8.07\%$ and $R_{WP} = 10.26\%$. Insets: schematic illustrations of the crystal structure (right) and the three-dimensional Mn-O_5 trigonal bipyramids (left) of $RMnO_3$ along the *ab* plane. Blue balls and red polyhedra represent the rare-earth atoms and Mn-O_5 trigonal bipyramids, respectively.

as a typical example in Fig. 2, illustrating that the calculated XRD pattern well matches the observed pattern. A summary of refinement results, including lattice parameters, atomic positions, and agreement factors, is given in Table I. The agreement factors of all the samples are no larger than $R_p = 10\%$ and $R_{wp} = 12.9\%$. Both calculated lattice parameters and structural data are in good line with another reported work.[17]

Figure 3(a) presents the Er doping variations of the lattice parameters a and c of the single-phase $Ho_{1-x}Er_xMnO_3$ compounds. The a lattice parameter decreases as the Er content increases, whereas the c lattice parameter, ranging from 11.39 to 11.42 Å, nearly keeps constant with pretty minor fluctuations. The decreases in the a lattice parameter is ascribed to the small ionic radius of Er^{3+} ions (103 pm) compared with that of Ho^{3+} ions (104.1 pm). The evolutions of *ab*-plane Mn-O3 and Mn-O4 bond lengths with the Er content are shown in Fig. 3(b). The Mn-O3 bond lengths show a general increasing trend from 1.96 Å for $x = 0$ to 2.22 Å for $x = 1$ with certain fluctuations. In contrast, the Mn-O4 bond lengths show a fluctuant decrease over a smaller range from 2.11 Å for $x = 0$ to 2.02 Å for $x = 1$. The Mn-O1 and Mn-O2 bond lengths along the c axis exhibit minor changes with doping, which are not shown here. In order to better understand variations of the crystal structure, the schematic illustrations of the crystal structure of $RMnO_3$ and Mn-O_5 trigonal bipyramids along the *ab* plane are shown in the inset of Fig. 2. In general, the Er doping does not notably affect the structure of the Mn-O_5 polyhedron, in agreement with the weak changes of the trigonal bipyramidal crystal field, which is proved by the fact that the Mn^{3+} ions ($3d^4$) remain in the high-spin state ($S = 2$) throughout the whole doping range.

TABLE I. Rietveld refinement summary for $Ho_{1-x}Er_xMnO_3$ ($x = 0$, 0.1, 0.2, 0.4, 0.7, 0.8, 0.9, and 1).

			$x = 0$		$x = 0.1$	$x = 0.2$	$x = 0.4$
			Ours	Ref.[a]			
a (Å)			6.1493	6.1518	6.1478	6.1445	6.1362
c (Å)			11.4165	11.4131	11.4154	11.4167	11.4137
Ho(1)	2a(0, 0, z)	z	0.27137	0.2831	0.27169	0.27156	0.27310
Ho(2)	4b($1/3$,$2/3$, z)	z	0.22964	0.2421	0.23184	0.23060	0.23146
Er(1)	2a(0, 0, z)	z			0.27169	0.27156	0.27310
Er(2)	4b($1/3$,$2/3$, z)	z			0.23184	0.23060	0.23146
Mn	6c(x, 0, 0)	x	0.32033	0.3332	0.31769	0.33055	0.32240
O(1)	6c(x, 0, z)	x	0.38237	0.3002	0.45263	0.72339	0.30540
		z	0.47656	0.1451	0.03661	0.03460	0.14987
O(2)	6c(x, 0, z)	x	0.64330	0.6433	0.64713	0.64259	0.64072
		z	0.33628	0.3231	0.32982	0.33016	0.32646
O(3)	2a(0, 0, z)	z	0.49553	0.4982	0.49074	0.49483	0.49244
O(4)	4b($1/3$,$2/3$, z)	z	0.02726	0.0372	0.02839	0.03046	0.02540
R_p (%)			9.668		9.638	8.597	8.926
R_{wp} (%)			12.29	10.1	12.454	11.084	11.512
χ^2			3.742		4.198	3.618	3.93
			x = 0.7		x = 0.8	x = 0.9	x = 1
						Ours	Ref. [a]
a (Å)			6.1211	6.1167	6.1158	6.1155	6.1215
c (Å)			11.3923	11.3888	11.3895	11.4060	11.4101
Ho(1)	2a(0, 0, z)	z	0.27310	0.27310	0.27310		
Ho(2)	4b($1/3$,$2/3$, z)	z	0.23060	0.23206	0.23206		
Er(1)	2a(0, 0, z)	z	0.27310	0.27310	0.27310	0.28720	0.2761
Er(2)	4b($1/3$,$2/3$, z)	z	0.23060	0.23206	0.23206	0.22952	0.2341
Mn	6c(x, 0, 0)	x	0.32240	0.32240	0.34991	0.31299	0.3441
O(1)	6c(x, 0, z)	x	0.29052	0.31782	0.30419	0.30540	0.2892
		z	0.15319	0.15617	0.17284	0.14873	0.1522
O(2)	6c(x, 0, z)	x	0.65149	0.63266	0.64330	0.65697	0.6452
		z	0.33260	0.33260	0.36074	0.30509	0.3271
O(3)	2a(0, 0, z)	z	0.47630	0.48655	0.46010	0.23119	0.4912
O(4)	4b($1/3$,$2/3$, z)	z	0.01700	0.02243	0.03314	0.01700	0.0251
R_p (%)			8.069	8.502	8.63	9.986	
R_{wp} (%)			10.261	10.665	11.118	12.879	7.9
χ^2			3.872	4.333	5.03	4.92	

[a]Reference 17.

Figure 4 shows the temperature dependence of the relative dielectric constant of $Ho_{1-x}Er_xMnO_3$($x = 0$, 0.1, 0.2, 0.4, 0.7, 0.8, 0.9, 1) at different frequencies of 40, 71, and 100 kHz. No previous data about high-temperature dielectric constant of the $Ho_{1-x}Er_xMnO_3$ system were ever reported except of $ErMnO_3$ measured at a fixed frequency,[9] to which the dielectric constant value of our $ErMnO_3$ sample is comparable. In the ε-T curve of $HoMnO_3$, the dielectric constant is independent of frequency and temperature, with a value of about 60 below 400 K. Once the temperature exceeds 400 K, the dielectric constants go up dramatically with strong dispersions, which are followed by a plateau with $\varepsilon \approx 310$ from 620 to 700 K. The drop-off temperature (T_m), where the dielectric constant on the plateau begins to reduce with decreasing temperatures, shifts towards higher temperatures as frequencies increase, indicating dielectric relaxation behavior in this compound. Above 750 K, the dielectric constants display a second sharp increase at higher temperatures. This is caused by enhanced current leakage, since grain boundaries have large conductivity and oxygen loss at high temperatures. Thus, large oxygen loss is responsible for the absence of high-temperature ferroelectric transitions in the temperature dependence of the dielectric constants, which occur in all as-prepared samples. $ErMnO_3$ shows similar relaxation behavior below 550 K. The plateau, with $\varepsilon \approx 270$, is extended over a temperature range from 550 to 700 K. The increase in the dielectric constants above 750 K is not so sharp as in $HoMnO_3$, indicative of different oxygen diffusion behavior at high temperatures. Regarding the other doped samples, strong relaxation behavior is also observed below $T = 480$ K. Thus, all single-phase $Ho_{1-x}Er_xMnO_3$ compounds possess a dielectric relaxation process. However, the temperature dependent dielectric constants of the doped samples have two differences from those of the two undoped samples. Firstly, the dielectric constant values of doped samples, except with $x = 0.4$, are much smaller than those of the $HoMnO_3$ and $ErMnO_3$ samples. Moreover, broad peaks appear instead of steplike decreases over a wide temperature range from 350 to 650 K. The dielectric relaxation processes mentioned above are also confirmed by corresponding frequency-dependent dielectric steps or

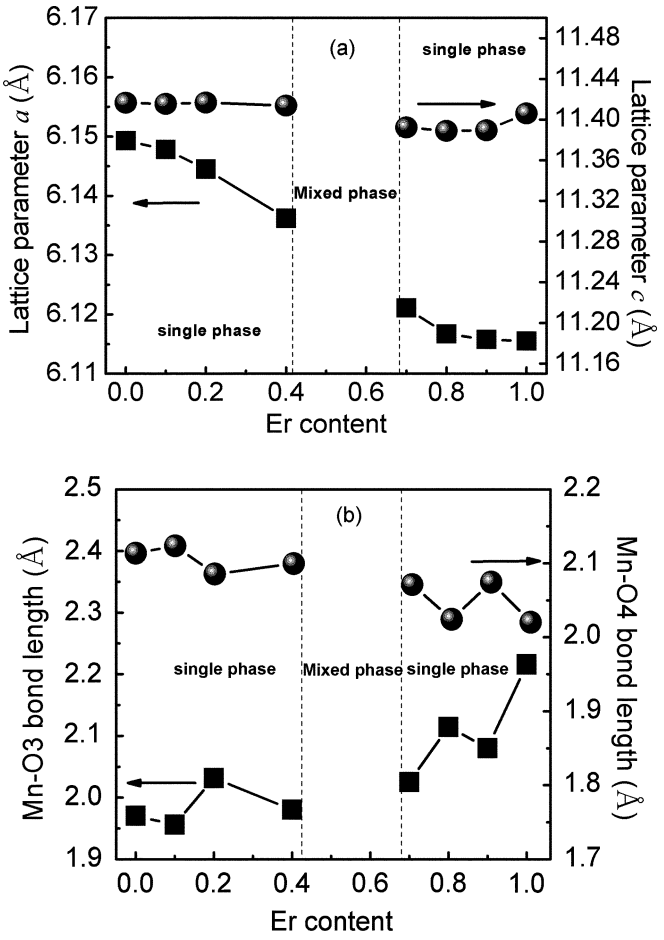

FIG. 3. (a) Evolutions of lattice parameters a and c of $Ho_{1-x}Er_xMnO_3$ ($x = 0$, 0.1, 0.2, 0.4, 0.7, 0.8, 0.9, 1) compounds with Er concentration. (b) The Er doping variations of the Mn-O3 and Mn-O4 bond lengths.

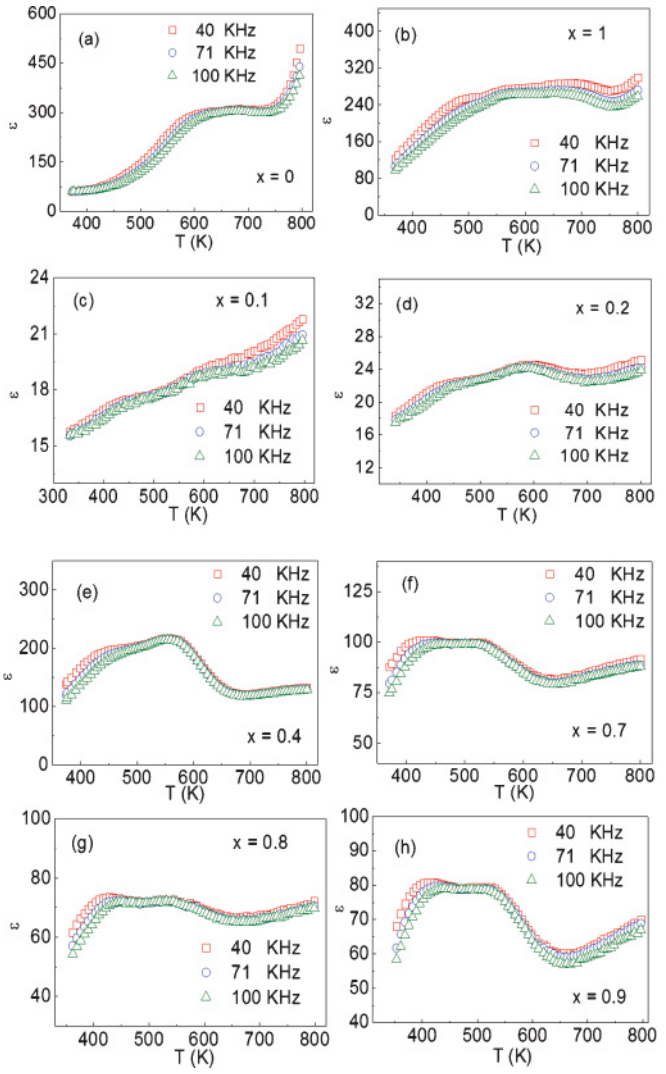

FIG. 4. (Color online) The temperature dependence of dielectric constant of $Ho_{1-x}Er_xMnO_3$ ($x = 0$, 0.1, 0.2, 0.4, 0.7, 0.8, 0.9, 1) at different frequencies.

broad peaks in the temperature dependence of the imaginary part of dielectric constant, which are shown in Fig. 5 with $Ho_{1-x}Er_xMnO_3$ ($x = 0$, 0.4, 0.7, and 1) as representative samples. The variations of drop-off temperatures (T_m) with frequencies are fitted with Arrhenius law $f = f_0 \exp(-E_0/K_B T_m)$, where E_0 is activation energy, K_B is the Boltzman parameter, and f_0 is the characteristic relaxation frequency at infinite temperature. As can been seen in the insets of Fig. 5, measured frequencies well obey the Arrhenius law with fitting parameters $f_0 = 2.91 \times 10^{15}$ Hz and $E_0 = 1.27$ eV for $HoMnO_3$, $f_0 = 6.20 \times 10^{11}$ Hz and $E_0 = 0.65$ eV for $Ho_{0.6}Er_{0.4}MnO_3$, $f_0 = 9.60 \times 10^{11}$ Hz and $E_0 = 0.62$ eV for $Ho_{0.3}Er_{0.7}MnO_3$, and $f_0 = 1.60 \times 10^{11}$ Hz and $E_0 = 0.64$ eV for $ErMnO_3$. These activation energy are reasonable compared with 0.98 eV for $Bi_{0.8}Ba_{0.2}Fe_{0.8}Mn_{0.2}O_3$,[18] 0.59 eV for $BaTiO_3$.[19] They are close to typical 1 eV of the oxygen vacancies mobility activation energy, suggesting the observed dielectric relaxation of the $Ho_{1-x}Er_xMnO_3$ system is induced by oxygen vacancies.

Ferroelectric hysteresis loops of $Ho_{1-x}Er_xMnO_3$ ($x = 0$, 0.2, 0.7, 1) compounds collected at the frequency of 1 kHz at room temperature are shown in Fig. 6. We did not observe saturation in these loops due to the leaky nature of ceramic samples. $HoMnO_3$ and $ErMnO_3$ are much leakier compared with $Ho_{0.8}Er_{0.2}MnO_3$ and $Ho_{0.3}Er_{0.7}MnO_3$. The remnant polarizations for $Ho_{1-x}Er_xMnO_3$ ($x = 0$, 0.2, 0.7, 1) compounds are 0.01, 0.004, 0.01, and 0.05 $\mu C/cm^2$, respectively, and the corresponding coercive fields are 7.10, 3.97, 6.45, and 8.45 kV/cm in sequence. The ferroelectric polarization values of as-prepared samples are small in contrast with thin films and those synthesized by pyrophoric reaction process.[9,20] Even though the hysteresis loops are small, they are still significant enough to definitely confirm the ferroelectricity of the $Ho_{1-x}Er_xMnO_3$ compounds.

Figure 7 presents the FC (field-cooled) χ-T curves of $Ho_{1-x}Er_xMnO_3$ ($x = 0$, 0.2, 0.4, 0.8, 1) under a magnetic field of 1000 Oe. These χ-T curves all show a paramagnetic-like behavior. The FC and zero-field cooled (ZFC) curves overlap over the whole temperature range, and no clear magnetic transition peaks are observed, similar to previous reports.[21] This is because the paramagnetism originating from the Ho^{3+} and Er^{3+} ions masks the antiferromagnetic moments from the

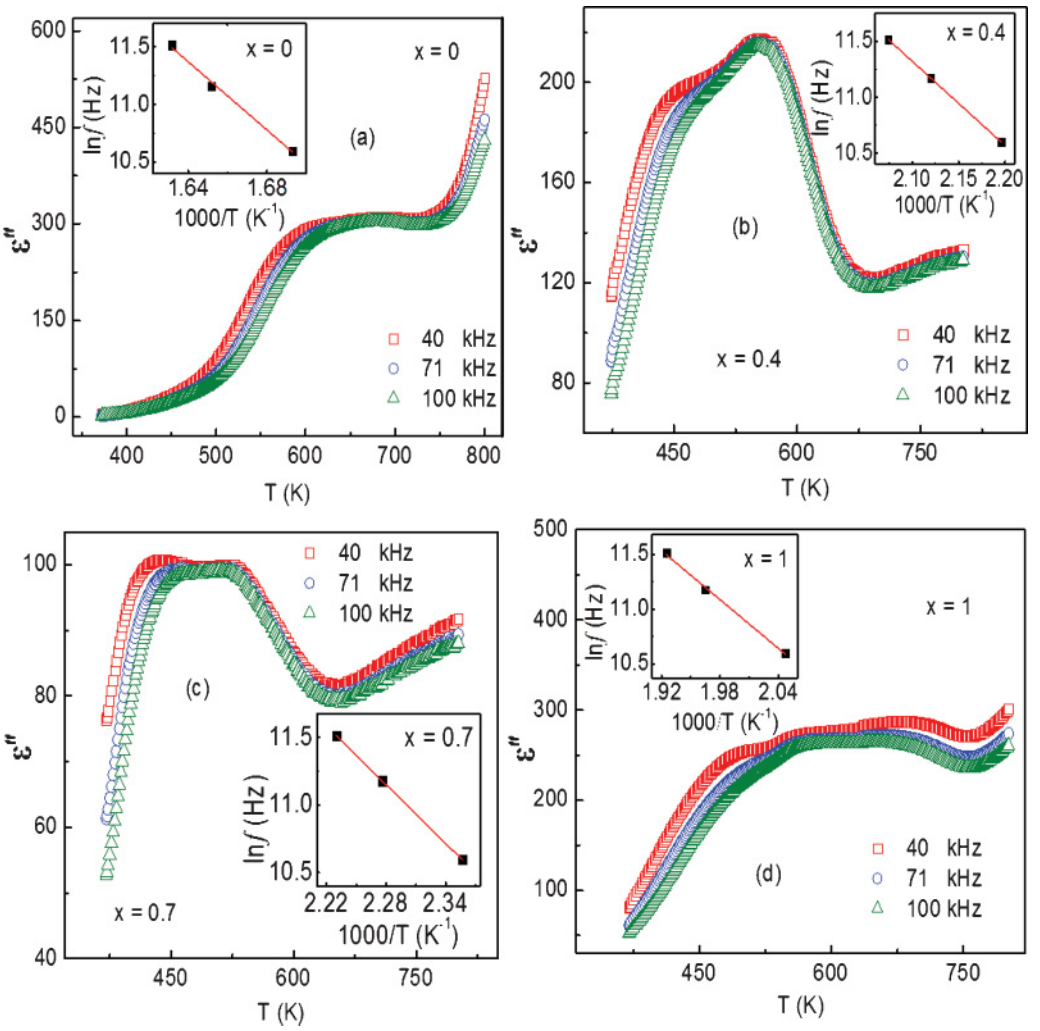

FIG. 5. (Color online) Variation of the imaginary part of dielectric constant of $Ho_{1-x}Er_xMnO_3$ ($x = 0$, 0.4, 0.7, 1) with temperature at different frequencies. Insets: Measured frequency as a function of $1000/T$, where square symbols are experimental points and solid lines are Arrhenius fittings.

Mn-Mn ordering. The inverse magnetic susceptibility data exhibit linear behavior above 100 K, as shown in Fig. 7. The Curie-Weiss temperatures (θ_{cw}) and effective magnetic moments were calculated based on linear parts according to the Curie-Weiss fitting. For example, the respective θ_{cw} values are -23 K for $ErMnO_3$ and -21 K for $HoMnO_3$, implying the existence of antiferromagnetic ordering below the Néel temperature (T_N). The experimental effective magnetic moments of the $Ho_{1-x}Er_xMnO_3$ ($x = 0$, 0.2, 0.4, 0.8, and 1) samples are 11.3, 11.1, 11.7, 10.5, and 10.4 μ_B, respectively, with μ_B the Bohr magneton, which are well consistent with the theoretical magnetic moments calculated from 10.6 μ_B for Ho^{3+} ($S = 2$, $J = 8$), 9.6 μ_B for Er^{3+} ($S = 3/2$, $J = 15/2$), and 4.9 μ_B for Mn^{3+} ($S = 2$). Thus Mn^{3+} ions ($3d^4$) in single-phase samples remain stable in the high-spin state. As the Mn^{3+} ions possess three energy levels in the trigonal bipyramidal crystal field, the d_z^2 orbitals of the high-spin Mn^{3+} ions are not occupied by any electrons. The Er doping at the Ho sites does not affect the crystal field of the Mn-O_5 polyhedron significantly, responsible for stability of the spin state of the Mn^{3+} ion.

The isothermal magnetization (M-H) curves of $Ho_{1-x}Er_xMnO_3$ ($x = 0$, 0.2, 0.4, 0.8, 1) measured at 10 K are shown in Fig. 8. The magnetizations of these samples increase linearly with increasing magnetic field below 20 kOe and do not saturate up to 50 kOe. As for $HoMnO_3$ and $ErMnO_3$, the magnetization at 50 kOe is 5.6 μ_B and 3.7μ_B, respectively, which is much smaller than the corresponding theoretical saturated values of 8 μ_B and 7 μ_B. Moreover, the magnetizations of these samples decrease according to the increasing erbium concentration, as a result of the smaller effective magnetic moment of Er^{3+} (9.6 μ_B) compared to Ho^{3+} (10.6 μ_B).

The temperature dependence of the specific heat (C_P) for the $Ho_{1-x}Er_xMnO_3$ ($x = 0$, 0.3, 0.5, 0.8, 1) samples was measured from 2 to 100 K without magnetic fields, as shown in Fig. 9. Our specific heat data is in good line with previous reports.[15,22] The characteristic λ-shape anomalies observed in all the samples are caused by the phase transition from a conventional second-order paramagnetic phase to an antiferromagnetic phase. As the Er content increases, the C_P anomaly peak position gradually shifts from 72 K for $HoMnO_3$

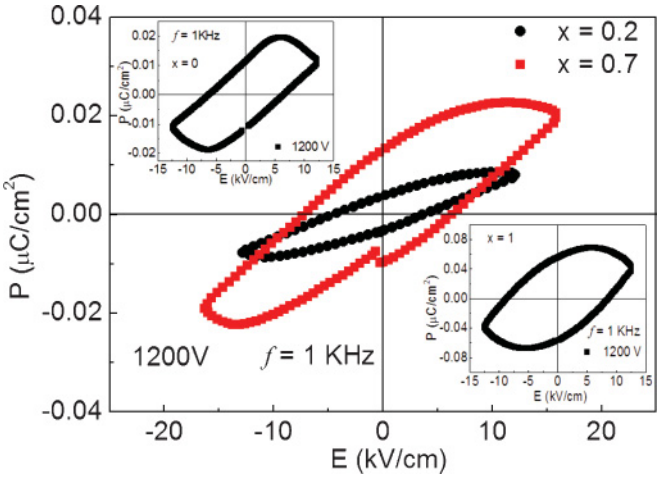

FIG. 6. (Color online) Ferroelectric hysteresis loops of $Ho_{1-x}Er_xMnO_3$ ($x = 0$, 0.2, 0.7, 1) at room temperature.

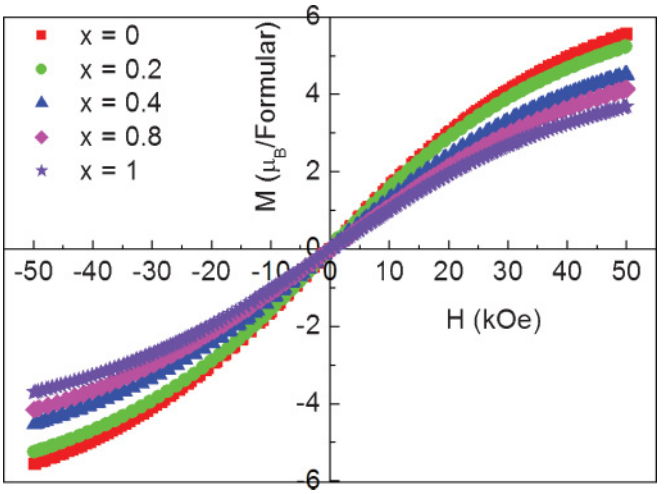

FIG. 8. (Color online) Isothermal magnetization curves of $Ho_{1-x}Er_xMnO_3$ ($x = 0$, 0.2, 0.4, 0.8, 1) at 10 K.

to 76 K for $ErMnO_3$, indicating that the increasing Er content enhances the antiferromagnetic transition temperature. It is noteworthy that two transition peaks at 72 and 76 K were observed in the sample with $x = 0.5$ due to the coexistence of $ErMnO_3$ and $HoMnO_3$ phases, supporting the analysis of XRD patterns. A small peak observed in $HoMnO_3$ at very low temperature (~12 K) is possibly ascribed to the antiferromagnetic ordering of the Ho^{3+} ions.[22] In order to study the excess magnetic heat capacity (ΔC_P), smooth backgrounds of lattice contribution to specific heat were extracted using a third-order polynomial fitting exclusive of the regions around T_N from the C_P-T data of $HoMnO_3$ and $ErMnO_3$, as illustrated in Fig. 10. In the upper left insets of Fig. 10, the magnetic entropy changes (ΔS_{Mag}) near T_N, corresponding to the variation of disordering around the transition from a paramagnetic state to an antiferromagnetic state, can be calculated from $\Delta S_{Mag} = \int_{T_1}^{T_2} \frac{\Delta C_p}{T} dT$, where T_1 and T_2 define a temperature range around T_N, e.g., $T_N \pm 25$ K. The calculated ΔS_{Mag} are 0.745 J/mol K for $ErMnO_3$ and 0.728 J/mol K for $HoMnO_3$, respectively. These ΔS_{Mag} values are comparable to 1.3 J/mol K for $ScMnO_3$ and 0.67 J/mol K for $La_{0.2}Ca_{0.8}MnO_3$.[16,23] The theoretical value of ΔS_{Mag}, known as the magnetic entropy changes for the transition from a paramagnetic state to a perfectly ordered state, is obtained through the equation of $\Delta S_{theo} = R \ln(2S + 1)$, where S is the spin number of Mn^{3+} ions in these samples and R is the molar gas constant. Thus, the calculated values are much smaller than the theoretical values of $R \ln 5 = 13.38$ J/mol K. The deviations are possibly as a result that either a larger proportion of the spin entropy is "located" at low temperature or short-range magnetic correlations persist to temperatures much higher than T_N.[23] The lower right insets show the curves in the low-temperature region (2 K < T < 30 K), which are fitted by $C_P(T) = \gamma T + \beta T^3$, where the γT term describes the electronic contribution to specific heat due to free charges and the βT^3 term describes the lattice contribution arising from lattice vibration. The Sommerfeld coefficient γ to identify the electronic linear term is given in a free-electron model by $\gamma = \pi^2 k_B^2 N(E_F)/3$, where $N(E_F)$ is the density of states at the Fermi level. The coefficient β of lattice con-

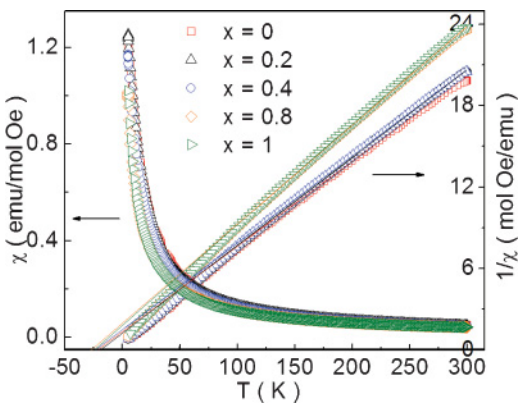

FIG. 7. (Color online) The temperature dependence of (a) magnetic susceptibilities and (b) inverse magnetic susceptibilities of $Ho_{1-x}Er_xMnO_3$ ($x = 0$, 0.2, 0.4, 0.8, 1) measured under the FC process in a magnetic field of 1000 Oe over a temperature range from 5 to 300 K.

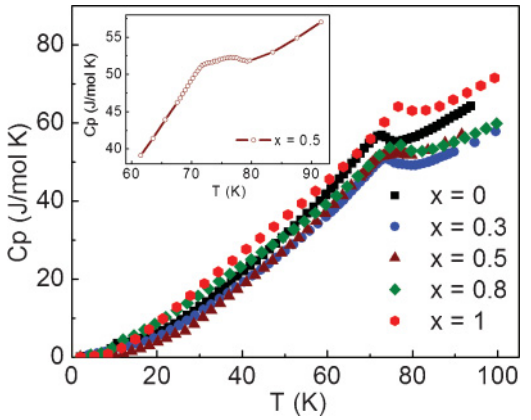

FIG. 9. (Color online) The temperature variation of specific heat capacities of $Ho_{1-x}Er_xMnO_3$ ($x = 0$, 0.3, 0.5, 0.8, 1). Inset shows the anomaly in the vicinity of T_N for the $x = 0.5$ sample.

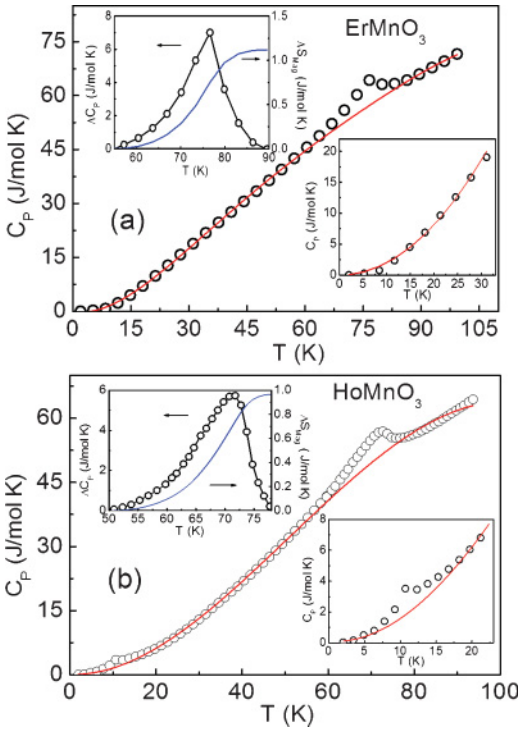

FIG. 10. (Color online) The temperature dependence of the heat capacity of (a) $ErMnO_3$ and (b) $HoMnO_3$. The red lines are the smooth backgrounds obtained with a third-order polynomial fitting. Upper left insets: the excess magnetic heat capacity (open circle symbols) of the compounds extracted from the heat capacity by subtracting the corresponding smooth backgrounds. Blue lines show the temperature dependence of the magnetic entropy. Lower right insets: the temperature dependence of the heat capacity over the temperature range from 2 to 30 K. Red lines represent the fitting with $C_P(T) = \gamma T + \beta T^3$.

tribution is given in the Debye model by $\beta = 234Nk_B/\Theta_D^3$, where N is the number of ions/mole and Θ_D is the Debye temperature that represents the effective cutoff phonon energy of materials. $ErMnO_3$ has $\gamma = 6 \times 10^{-6}$ J/mol K^2 and $\beta = 3.5 \times 10^{-5}$ J/mol K^4, while $HoMnO_3$ has $\gamma = 0.038$ J/mol K^2 and $\beta = 1.29 \times 10^{-4}$ J/mol K^4. As the density of charge carriers is proportional to the value of γ, the current leakage of $HoMnO_3$ is larger than that of $ErMnO_3$, consistent with observations from ferroelectric hysteresis loops. It is also proven that the $HoMnO_3$ and $ErMnO_3$ samples synthesized by solid-state reaction method are dielectric materials with distinct current leaky nature. The Debye temperatures Θ_D are 381 K for $ErMnO_3$ and 422 K for $HoMnO_3$. These calculated values agree well with other reported work.[24]

IV. CONCLUSIONS

Single-phase $Ho_{1-x}Er_xMnO_3$ ($0 \leqslant x \leqslant 0.4$ and $0.7 \leqslant x \leqslant 1$) compounds were synthesized by the solid-state reaction method. The decreases in the a lattice parameter with increasing Er content are caused by the small ionic radius of the Er^{3+} ions. All the samples are ferroelectric materials not only with a current leaky nature, but also with dielectric relaxation related to oxygen vacancies. Nevertheless, the high oxygen loss at high temperature prevents the appearance of high-temperature ferroelectric transition peaks in the dielectric constant data. The weakening magnetizations of the samples with the higher Er doping levels are due to smaller magnetic moments of the Er^{3+} ions compared to those of the Ho^{3+} ions; meanwhile the Mn^{3+} ions remain stable in the high-spin state. The antiferromagnetic transitions, which cannot be observed in the magnetic susceptibility data, are confirmed in the specific heat measurements, where the T_N gradually shifts from 72 K for $HoMnO_3$ to 76 K for $ErMnO_3$.

ACKNOWLEDGMENTS

X.L.W. thanks the Australian Research Council for support through Discovery projects DP0987190 and DP0558753.

*xiaolin@uow.edu.au

[1] H. Sugie, N. Iwata, and K. Kohn, J. Phys. Soc. Jpn. **71**, 1558 (2002).
[2] B. B. Van Aken, T. T. M. Palstra, A. Filippetti, and N. A. Spaldin, Nat. Mater. **3**, 164 (2004).
[3] N. A. Spaldin and M. Fiebig, Science **309**, 391 (2005).
[4] Z. X. Cheng, X. L. Wang, S. X. Dou, H. Kimura, and K. Ozawa, Phys. Rev. B **77**, 092101 (2008).
[5] W. C. Koehler, H. L. Yakel, E. O. Wollan, and J. W. Cable, Phys. Lett. **9**, 93 (1964).
[6] B. Lorenz, A. P. Litvinchuk, M. M. Gospodinov, and C. W. Chu, Phys. Rev. Lett. **92**, 087204 (2004).
[7] B. B. Van Aken, A. Meetsma, and T. T. M. Palstra, Acta Cryst. E **57**, i38 (2001).
[8] H. L. Yakel and W. C. Koehler, Acta Crystallogr. **16**, 957 (1963).
[9] P. Dey, T. K. Nath, and M. L. Nanda Goswami, Appl. Phys. Lett. **90**, 162510 (2007).
[10] S. B. Kim, S. J. Kim, J. G. Park, S. W. Cheong, and C. S. Kim, J. Appl. Phys. **99**, 08Q313 (2006).
[11] N. Iwata and K. Kohn, Ferroelectrics **219**, 161 (1998).
[12] F. Yen, C. R. Dela Cruz, B. Lorenz, Y. Y. Sun, Y. Q. Wang, M. M. Gospodinov, and C. W. Chu, Phys. Rev. B **71**, 180407 (2005).
[13] M. Fiebig, C. Degehardt, and R. V. Pisarev, Phys. Rev. Lett. **88**, 027203 (2002).
[14] H. D. Zhou, R. Vasic, J. Lu, J. S. Brooks, and C. R. Wiebe, J. Phys.: Condens. Matter **20**, 035211 (2008).
[15] M. C. Sekhar, S. Lee, G. Choi, C. Lee, and J. G. Park, Phys. Rev. B **72**, 014402 (2005).
[16] A. Muñoz, J. A. Alonso, M. J. Martínez-Lope, M. T. Casáis, J. L. Martínez, and M. T. Fernandez-Diaz, Chem. Mater. **13**, 1497 (2001).
[17] K. Uusi-Esko, J. Malm, N. Imamura, H. Yamauchi, and M. Karppinen, Mater. Chem. Phys. **112**, 1029 (2008).
[18] L. H. Yin, W. H. Song, X. L. Jiao, W. B. Wu, X. B. Zhu, Z. R. Yang, J. M. Dai, R. L. Zhang, and Y. P. Sun, J. Phys. D: Appl. Phys. **42**, 205402 (2009).
[19] S. Shirasaki, H. Yamamura, H. Haneda, K. Kakegawa, and J. Moopi, J. Chem. Phys. **73**, 4640 (1980).

[20]D. H. Kang, J. H. Chae, and E. S. Kim, J. Electroceram. **21**, 831 (2008).
[21]K. Yoshii and H. Abe, J. Solid State Chem. **165**, 131 (2002).
[22]I. Radulov, V. Lovchinov, D. Dimitrov, and P. Simeonova Ph. Vanderbemden, J. Optoelectron. Adv. Mater. **11**, 1553 (2009).
[23]V. Markovich, J. Wieckowski, M. Gutowska, A. Szewczyk, A. Wisniewski, C. Martin, and G. Gorodetsky, J. Appl. Phys. **107**, 063907 (2010).
[24]D. G. Tomuta, S. Ramakrishnan, G. J. Nieuwenhuys, and J. A. Mydosh, J. Phys. Condens. Matter **13**, 4543 (2001).